

Simulations of a Reconstructed Cerebellar Purkinje Cell Based on Simplified Channel Kinetics

Paul C. Bush

Terrence J. Sejnowski

Howard Hughes Medical Institute and Computational Neurobiology Laboratory,
The Salk Institute, La Jolla, CA 92037, USA

and

University of California at San Diego, La Jolla, CA 92037, USA

When cerebellar Purkinje cells are depolarized with a constant current pulse injected at the soma, complex spike discharge patterns are observed (Llinas and Sugimori 1980b). A computer model has been constructed to analyze how the Purkinje cell ionic conductances identified to date interact to produce the observed firing behavior. The kinetics of voltage-dependent conductances used in the model were significantly simpler than Hodgkin-Huxley kinetics, which have many parameters that must be experimentally determined. Our simplified scheme was able to reproduce the complex nonlinear responses found in real Purkinje cells. A similar approach could be used to study the wide variety of neurons found in different brain regions.

1 Introduction

Neurons have a wide range of shapes, sizes, and intrinsic properties, and have correspondingly specialized functions. In particular, dozens of nonlinear membrane conductances have been characterized that are found in different combinations at different spatial locations. These segregated nonlinear mechanisms, coupled with complex dendritic morphologies, make it possible in principle for single neurons to compute spatiotemporal correlations of very high order. A large network of semilinear processing units, familiar in connectionist models, would be needed to provide equivalent computational power.

Cerebellar Purkinje cells have large, complex dendritic trees with a variety of active membrane conductances inhomogeneously distributed over the dendrites and soma. *In vitro* intrasomatic and intradendritic recordings have been used to characterize these conductances (Llinas *et al.* 1980b; Llinas and Sugimori 1980a; Hounsgaard and Midtgaard 1988). The question of whether these conductances are sufficient to account for the observed responses of Purkinje cells can be addressed by incorporating them into compartmental models of reconstructed neurons.

Table 1: Rate Constants.

$C_m = 1 \mu\text{F}/\text{cm}^2$	$r_a = 225 \text{ -cm}$
Soma $g_{\text{leak}} = 1.32 \text{ mS}/\text{cm}^2$	Dendritic $g_{\text{leak}} = 0.0219 \text{ mS}/\text{cm}^2$
$g_{\text{Na}} = 40 \text{ mS}/\text{cm}^2$	$g_{\text{Kd}} = 2 \text{ mS}/\text{cm}^2$
$g_{\text{Nap}} = 0.25 \text{ mS}/\text{cm}^2$	$g_{\text{Ca}} = 2 \text{ mS}/\text{cm}^2$
$g_{\text{K}} = 2 \text{ mS}/\text{cm}^2$	$g_{\text{Cas}} = 0.03 \text{ mS}/\text{cm}^2$
$g_{\text{Kca}} = 0.1 \text{ mS}/\text{cm}^2$	Resting $[\text{Ca}]_i = 50 \text{ nM}$
$[\text{Ca}]_i$ decay rate = 5 msec^{-1}	

	V_θ (mV)	R_α (msec $^{-1}$ mV $^{-1}$)	R_β (msec $^{-1}$)	R_δ (msec $^{-1}$)	γ (msec $^{-1}$)
g_{Na}	-50	0.13	0	0.1	7
g_{Kd}	-50	0.08	0.05	0.1	0.1
g_{Nap}	-57	0.0009	0.005	0	0
g_{Ca}	-30	0.06	0.05	0.1	5
g_{K}	-30	0.04	0.02	0	0
g_{Cas}	-55	0.0006	0.01	0	0
g_{Kca}	-55	$\alpha = 100 \times [\text{Ca}]_i$	0.07	0	0

Unfortunately, the parameters that characterize Hodgkin-Huxley channel kinetics are often incomplete or inadequate. In this paper we adopt a simpler kinetic scheme that is much easier to fit to existing data and accurately captures the essential intrinsic properties of the channels.

The simplified kinetic scheme introduced here has the additional advantage that it allows accurate simulations of realistic neurons to be run much faster than with Hodgkin-Huxley kinetics that have multiple closed states. This speedup is important when many neurons must be simulated simultaneously in model neural networks.

2 Methods

The compartmental modeling technique has been well studied and can be used to explore the electrotonic properties of morphologically accurate neuron models (Rall 1964; Jack *et al.* 1975; Segev *et al.* 1989). Our simulations were based on a single cerebellar Purkinje cell reconstructed by Shelton (1985) (Fig. 1). The model consisted of 1089 compartments that contained active conductances consistent with data from the literature. The passive membrane parameters used in the model were those used by Shelton (Table 1). Note that the membrane resistance of the soma was $60\times$ lower than that of the dendrites.

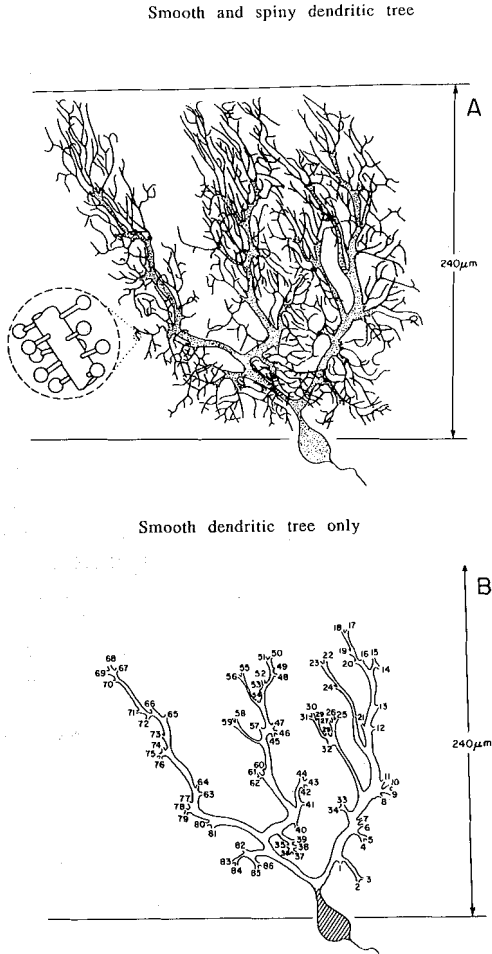


Figure 1: Morphology of rat cerebellar Purkinje cell (reprinted with permission from Shelton 1985). (A) Soma and proximal (smooth) dendrites are stippled. Spiny dendrites are drawn as lines. (B) Smooth dendritic tree only. Spiny dendritic tree attachments are numbered counterclockwise. Soma is hatched. The soma contains potassium and sodium conductances, smooth dendrites contain fast calcium and potassium conductances, and spiny dendrites contain slow calcium and potassium conductances (see text).

The soma contains a fast, inactivating sodium conductance, g_{Na} , responsible for the upstroke of the action potential, a fast potassium conductance, g_{Kd} , responsible for AP repolarization, and a low-threshold, slow, plateau sodium conductance, g_{Nap} . There are large, fast calcium conductances, g_{Ca} on the proximal (smooth) dendrites that cause discrete dendritic calcium spikes. These calcium spikes are repolarized by large potassium conductances, g_K . The spiny dendrites contain smaller, slower calcium conductances, g_{Cas} , and a slow calcium-dependent potassium conductance, g_{Kca} . See Table 1 for conductance values, g_x .

The Hodgkin-Huxley model of the squid axon is the starting point for most biophysical models of neurons (Hodgkin and Huxley 1952). The time- and voltage-dependent kinetics of the ionic conductances can be depicted as a Markov process (Hille 1984) (Fig. 2a). The following equations describe the transitions between the open/closed states, m , and the active/inactive states, h .

$$\begin{aligned}\frac{dm}{dt} &= \alpha(1 - m) - \beta m \\ \frac{dh}{dt} &= \gamma(1 - h) - \delta h\end{aligned}$$

In the Hodgkin-Huxley system the inactivation of the channel is independent of its activation. It is generally assumed that the rate constant of channel activation, α , is much larger than that of inactivation, γ . That is, channel opening is fast and channel closing (inactivation) is slow, so the decay of the macroscopic current is governed by γ . However, single channel patch clamp data from mammalian sodium channels (Aldrich *et al.* 1983) indicates that inactivation follows activation after a very short latency in a voltage-independent step. Thus, inactivation is coupled to activation, γ is not dependent on voltage and is much larger than the activation rate constant. The decay of the macroscopic current is governed by α (slow activation). These changes are incorporated into the model kinetics (Fig. 2b). Note that the same macroscopic current can be produced by different microscopic kinetics (Hille 1984; Kienker 1989). In our model it is assumed that there are no transitions from the inactivated to the open state or from the closed to the inactivated state. For conductances that do not inactivate the kinetics are reduced to a two-state system with two voltage-dependent rate constants. The following equations describe the state transitions of our model kinetics.

$$\begin{aligned}\frac{dC}{dt} &= \beta O - \alpha C + \delta X \\ \frac{dO}{dt} &= \alpha C - \beta O - \gamma O \\ X &= 1 - (C + O)\end{aligned}$$

as shown in Figure 2b.

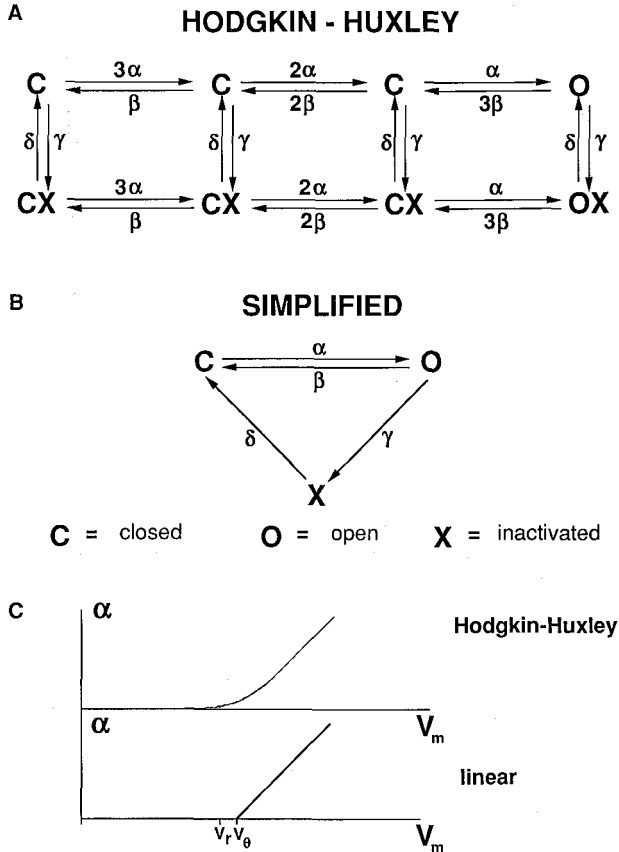


Figure 2: (A) Hodgkin-Huxley kinetics for the spike sodium conductance represented as a Markov process. Activation and inactivation are independent processes. (B) The simplified kinetics used in our model (derived from Aldrich *et al.* 1983). Inactivation is coupled to activation with a voltage-independent step. There are no transitions from the inactivated state to the open state nor from the closed to the inactivated state. See text for the equations describing the voltage-dependent transitions between the states. These kinetics were used for all conductances in the model. (C) The voltage dependence of the Hodgkin-Huxley activation rate constant is shown above, and the linear simplification used in our model is shown below.

In the traditional Hodgkin–Huxley model of the sodium channel the rate constants α , β , γ , and δ are determined empirically by fitting voltage-clamp data with equations of the form

$$f(V_m) = \frac{A(B + V_m)}{C + e^{(D+V_m)/F}}$$

Where the constants A , B , C , D , and F are different for each rate constant. A very accurate fit to current clamp data can be obtained provided complete voltage clamp data are available for the conductance in question. If complete data are not available then it is difficult to modify an existing set of Hodgkin–Huxley conductance parameters to obtain even slightly different behavior. In our model the rate constants are directly or inversely proportional to voltage, V_m (Fig. 2c).

$$\alpha = \begin{cases} 0 & \text{if } V_m \leq V_\theta \\ (V_m - V_\theta)R_\alpha & \text{if } V_m > V_\theta \end{cases}$$

$$\beta, \delta = \begin{cases} R_{\beta, \delta} & \text{if } V_m \leq V_\theta \\ [1 \text{ mV}/(V_m - V_\theta)] R_{\beta, \delta} & \text{if } V_m > V_\theta \end{cases}$$

where voltages are in millivolts. The rate constants β and δ were constrained to be less than or equal to $R_{\beta, \delta}$ at all times. Since the threshold V_θ for each conductance is fairly easy to establish from current clamp data, adjusting the rate constants is just a matter of varying the slope of their voltage dependence, R_x (Table 1). Thus it is easy to fit the behavior of the conductance to any desired form. α is the most important parameter as it is the primary determinant of the activation and decay rates of the conductance transient. A large β reduces the activation rate and steady-state conductance, while a large δ prolongs the duration of an inactivating conductance transient. An inactivating conductance with a small δ takes a long time to recover after activation, and so does not function well at high frequencies.

The linear simplification of the rate constants inevitably reduces the accuracy of the model kinetics. However, the original Hodgkin–Huxley model was formulated to describe the conductances underlying the action potential, an invariable event produced by conductances unchanged from cell to cell. Conductances with longer time constants, responsible for determining the excitability and interspike intervals of the cell, are much more variable between cells and even within the same cell over time. In practice, the general behavior of each conductance in our model was well captured by a system with linear rate constants, a system that is computationally both simple and fast.

The calcium-dependent potassium conductance is not voltage dependent. The activation rate constant for this conductance in our model was proportional to intracellular calcium concentration rather than voltage. Calcium entry into a compartment was calculated from the calcium

current. Intracellular calcium decayed exponentially to the resting value (Table 1).

Under voltage clamp the activation of many ionic currents is sigmoidal with respect to time. To model this in the Hodgkin-Huxley system, the activation state variable (m) is raised to a power when calculating the ionic current (I), simulating closed-state transitions.

$$I = g_x m^3 h (E_r - V_m)$$

where E_r is the reversal potential and g_x is the maximum conductance of the ionic current.

This could be accomplished in our model by adding extra closed states, but this would add an extra step to the calculations, and would add extra rate constants that would be hard to constrain with existing physiological data. Consequently, in our model the ionic current is calculated as follows.

$$I = g_x O (E_r - V_m)$$

We simulated this compartmental model using CABLE, written by Michael Hines (Hines 1989) and further modified by Jack Wathey and William Lytton. The simulations were run on a MIPS RC3240. Simulation of 100 msec of model time required about 5 min of computation.

3 Results and Discussion

As a preliminary test of our simplified channel kinetics, we compared data from mammalian sodium current transients in response to various voltage steps (Aldrich *et al.* 1983) with the simulated sodium current transients of our model ($V_\theta = -50$ mV, $R_\alpha = 0.04$ msec⁻¹ mV⁻¹, $R_\beta = 0$ msec⁻¹, $R_\delta = 0.05$ msec⁻¹, $\gamma = 10$ msec⁻¹). The model reproduced the physiological data except for the slow rise phase of the current at low depolarizations (Fig. 3). This slow (sigmoidal) rise is due to transitions between closed states not included in the model, as discussed in the methods. However, leaving multiple closed states out of the model did not prevent us from achieving a close fit between the model Purkinje cell responses and the *in vitro* data (see below).

Figure 4A shows an intracellular recording from the soma of a turtle cerebellar Purkinje cell in response to a somatically injected depolarizing current (Hounsgaard and Midtgaard 1988). Although the dendritic morphology of the turtle Purkinje cell is not as complex as that of mammalian Purkinje cells, the firing pattern is not significantly different (Llinas and Sugimori 1980b). This indicates that the firing pattern is not dependent on the exact morphology of the neuron.

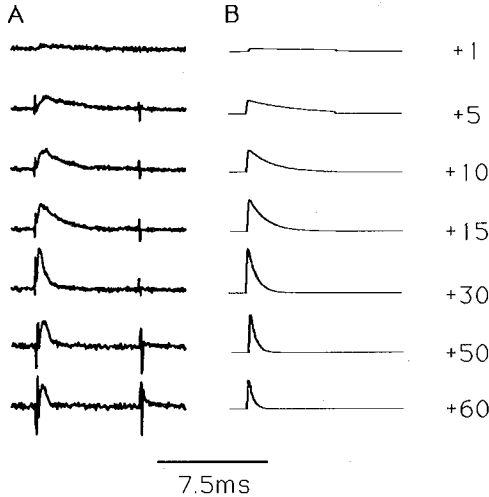


Figure 3: Voltage clamp responses of mammalian and model sodium spike conductances. (A) Averaged single channel currents for steps to different command voltages (shown as millivolts above threshold on the right) (reprinted with permission from Aldrich *et al.* 1983). (B) Responses of model sodium conductance to same voltage steps as in (A). The increased peak height and faster decay of the current transient with depolarization are common to both the model and the physiology, as is the decrease of the peak height as the command voltage approaches the sodium reversal potential (last two traces). The model, however, does not show the slow rise of the current transient seen at low depolarizations by the real cell. The slow rise is due to voltage-dependent transitions between closed states, which are not included in the model. Time scale bar is 7.5 msec for all traces except top trace, for which it is 15 msec.

Figure 4B shows the response of the model to a simulated somatic injection of depolarizing current, recorded at the soma. The pattern of spikes is similar to that displayed by real Purkinje cells in response to depolarizing current (Fig. 4A): A slow depolarization due to sodium and calcium plateau currents causes an accelerating train of sodium-dependent action potentials at the soma. A high-threshold calcium-dependent spike is triggered in the dendrites just at the point of inactivation of the sodium spike train. Voltage- and calcium-dependent potassium currents then produce a large hyperpolarization, which deactivates the sodium spikes, allowing the cycle to begin again. After the depolarizing current is turned off there is an "afterdischarge" of spikes due to residual activation of the plateau currents.

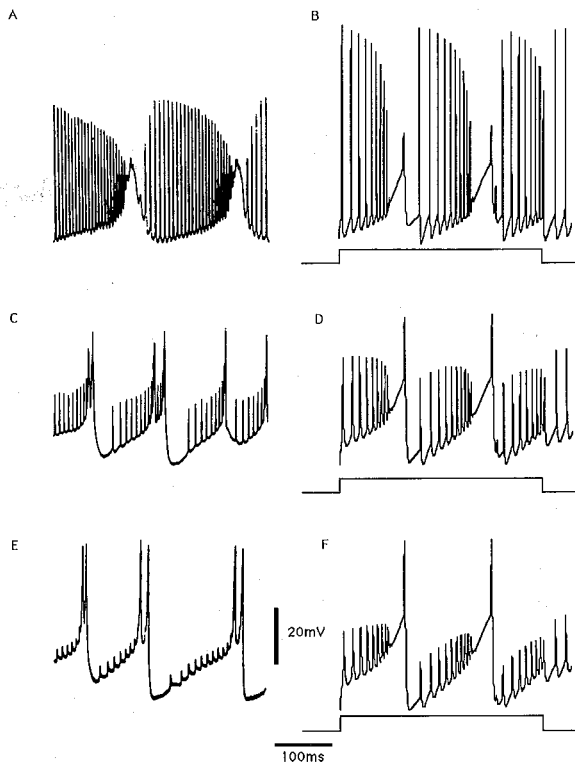


Figure 4: Intracellular recordings from a turtle cerebellar Purkinje cell in response to a somatically injected constant depolarizing current pulse are shown on the left (reprinted with permission from Hounsgaard and Midtgaard 1988). (A) Recording from the soma. Somatic sodium spikes ride on a slow depolarization due to plateau currents. When sodium spikes are voltage inactivated the membrane potential reaches the threshold of the dendritic calcium spike conductance. The resulting calcium spike is repolarized by potassium conductances, which resets the sodium spiking. (C,E) Recordings from proximal and distal dendrites, respectively. The small size of the sodium spikes and relatively large calcium spikes reflect their respective sites of generation. (B,D,F) Model responses from soma and proximal and distal dendrites, respectively, are shown on the right. The model replicates all the essential features of Purkinje cell behavior. The duration of the stimulus is shown beneath each trace. Firing continues after the stimulus is turned off due to the continued activation of plateau currents, as seen in real cells (Llinas *et al.* 1980b).

Figure 4C, D and E, F show comparisons between intracellular recordings and model recordings in a proximal dendrite and a distal dendrite, respectively. The sodium spikes become smaller as they passively propagate into the dendrites, confirming their somatic origin. The calcium spikes are much larger in the dendrites than the soma, reflecting their site of generation. The calcium spikes of the model are not the "doublets" seen in real cells. It is possible that these multiple spikes are the result of inhomogeneities in the density of calcium channels over the proximal dendrites (Llinas and Sugimori 1980b). The calcium channels responsible for the spiking in the model were homogeneously distributed over the proximal dendrites. Our model was not designed to address questions concerning the detailed spatial localization of channels or the subtleties of intradendritic calcium dynamics. Instead it is aimed at developing "unit cells" for use in physiologically realistic network models. If some of these properties are later found to be important for information processing (as they are likely to be) then the model can be modified appropriately.

We expect that the spiking pattern displayed by our model could be reproduced by a geometrically simplified neuron (Bush and Douglas 1991), though not if the model were reduced to just a single compartment. Such a simplification would significantly increase the speed of the model, which would be important for network simulations incorporating many such neurons.

Although no "A"-like potassium conductance was explicitly included in the model, we found that to allow the depolarization to continue to calcium spike threshold after inactivation of the sodium spikes, it was necessary to make the delayed rectifier potassium conductance inactivate slowly with depolarization. This is the essential characteristic of the "A" conductance (Connor and Stevens 1971). Thus the model predicts that the Purkinje cell delayed rectifier responsible for repolarization after a sodium spike has "A"-like properties.

4 Conclusion

Our model builds on previous models of Purkinje cells (Shelton 1985; Segev et al. 1991). The model demonstrates that the conductances characterized to date are sufficient to produce the cyclical firing pattern generated by Purkinje cells in response to constant depolarizing current input.

The channel kinetics used in the model, differing significantly from Hodgkin-Huxley kinetics, are useful in fitting complex response functions due to many incompletely characterized conductances. These simplified kinetics can be rapidly and easily tuned to simulate the intrinsic behavior of any neuron. Such single neuron models can then be incorporated into model networks where speed and simplicity of operation are more important characteristics of the component neurons than the detailed performances of their ionic conductances. These models

would also be easier to analyze with phase planes than would full-scale Hodgkin-Huxley models.

Acknowledgments

This work was started at the "Methods in Computational Neuroscience" MBL short course taught by James Bower and Christof Koch. We thank Tony Bell, Paul Rhodes, and Shawn Lockery for helpful discussions and technical assistance.

References

- Aldrich, R. W., Corey, D. P., and Stevens, C. F. 1983. A reinterpretation of mammalian sodium channel gating based on single channel recording. *Nature (London)* **306**, 436-441.
- Bush, P. C., and Douglas, R. J. 1991. Synchronization of bursting action potential discharge in a model network of neocortical neurons. *Neural Comp.* **3**(1), 19-30.
- Connor, J. A., and Stevens, C. F. 1971. Voltage clamp studies of a transient outward membrane current in gastropod neural somata. *J. Physiol.* **213**, 21-30.
- Hille, B. 1984. *Ionic Channels of Excitable Membranes*. Sinauer Associates, Sunderland, MA.
- Hines, M. L. 1989. A program for simulation of nerve equations with branching geometries. *Int. J. Biomed. Comp.* **24**, 55-68.
- Hodgkin, A. L., and Huxley, A. F. 1952. A quantitative description of membrane current and its application to conduction and excitation in nerve. *J. Physiol.* **117**, 500-544.
- Hounsgaard, J., and Midtgaard, J. 1988. Intrinsic determinants of firing pattern in Purkinje cells of the turtle cerebellum in vitro. *J. Physiol.* **402**, 731-749.
- Jack, J. J. B., Noble, D., and Tsien, R. W. 1975. *Electric Current Flow in Excitable Cells*. Oxford University Press, Oxford.
- Kienker, P. 1989. Equivalence of aggregated Markov models of ion-channel gating. *Proc. R. Soc. Lond. B* **236**, 269-309.
- Llinas, R., and Sugimori, M. 1980a. Electrophysiological properties of in vitro Purkinje cell dendrites in mammalian cerebellar slices. *J. Physiol.* **305**, 197-213.
- Llinas, R., and Sugimori, M. 1980b. Electrophysiological properties of in vitro Purkinje cell somata in mammalian cerebellar slices. *J. Physiol.* **305**, 171-195.
- Rall, W. 1964. Theoretical significance of dendritic tree for input-output relation. In *Neural Theory and Modeling*, R. Reiss, ed., pp. 73-97. Stanford University Press, Stanford.
- Segev, I., Fleshman, J. W., and Burke, R. E. 1989. Compartmental models of complex neurons. In *Methods in Neuronal Modeling: From Synapse to Networks*, C. Koch and I. Segev, eds., pp. 63-96. MIT Press, Cambridge, MA.

- Segev, I., Rapp, M., Manor, Y., and Yarom, Y. 1991. Analog and digital processing in single nerve cells: dendritic integration and axonal propagation. In *Single Neuron Computation*, T. McKenna, J. Jarvis, and S. F. Zarnetzer, eds. Academic Press, New York.
- Shelton, D. P. 1985. Membrane resistivity estimated for the Purkinje neuron by means of a passive computer model. *Neurosci.* **14**, 111-131.

Received 17 January 1991; accepted 22 April 1991.